Coherent-strained superconducting $BaPb_{1-x}Bi_xO_3$ thin films by interface engineering

Jinkwon Kim,[1,2] Junsik Mun,[3] Bongju Kim,[1,2] Han Gyeol Lee,[1,2] Daesu Lee,[1,2] Tae Heon Kim,[4] Shinbuhm Lee,[5] Miyoung Kim,[3] Seo Hyoung Chang,[6,*] and Tae Won Noh[1,2,†]

[1]*Center for Correlated Electron Systems, Institute for Basic Science (IBS), Seoul 08826, Republic of Korea*
[2]*Department of Physics and Astronomy, Seoul National University, Seoul 08826, Republic of Korea*
[3]*Department of Materials Science and Engineering and Research Institute of Advanced Materials, Seoul National University, Seoul 08826, Republic of Korea*
[4]*Department of Physics, University of Ulsan, Ulsan 44610, Republic of Korea*
[5]*Department of Emerging Materials Science, Daegu-Gyeongbuk Institute of Science and Technology, Daegu 42988, Republic of Korea*
[6]*Department of Physics, Chung-Ang University, Seoul 06974, Republic of Korea*

(Received 22 June 2019; published 21 November 2019)

The bismuthate superconductor $BaPb_{1-x}Bi_xO_3$ and its bismuthate heterostructure have gained much attention due to their potential applications, such as topologically protected quantum devices. To fabricate $BaPb_{1-x}Bi_xO_3$-based junctions or devices with atomically sharp interfaces, researchers have long searched for innovative methods to achieve coherent-strained superconducting $BaPb_{1-x}Bi_xO_3$ films. However, the large lattice mismatches between $BaPb_{1-x}Bi_xO_3$ and widely used perovskite substrates have been huge obstacles hindering the achievement of coherent-strained superconducting films. Here, we successfully fabricated coherent-strained superconducting $BaPb_{1-x}Bi_xO_3$ films on $SrTiO_3$ substrates by inserting $BaCeO_3/BaZrO_3$ buffer layers. By performing both grazing-incidence in-plane x-ray diffraction and transmission electron microscopy, we demonstrated that without buffer layers the $BaPb_{1-x}Bi_xO_3$ films exhibited fully relaxed structures with a reconstructed interface layer. With buffer layers, the superconducting transition temperatures of coherent-strained $BaPb_{1-x}Bi_xO_3$ films were higher than that of relaxed films. Based on these interface-engineering results, this paper provides opportunities for exploring the emergent properties of bismuthate-based superconducting devices, such as quantum computing circuits.

DOI: 10.1103/PhysRevMaterials.3.113606

I. INTRODUCTION

Perovskite oxide heterostructures often exhibit emergent physical properties, e.g., two-dimensional electronic gas [1], superconductivity (SC) [2,3], multiferroics [4], and magnetism [5]. Recently, spin-orbit interactions and topological physics in oxide heterostructures have given rise to promising methods for creating novel electronic and quantum devices based on interfaces or junctions [6–11]. For example, interfaces composed of topological insulators (TIs) and conventional superconductors are theoretically predicted to host Majorana bound states [12], which could be useful for new types of quantum computing circuits. To realize junction-based topological devices, coherent-strained films with atomically sharp interfaces are required.

Bismuthate heterostructures are promising platforms for exploring the possibilities of the theoretically predicted TI phases [7,8] as well as for investigating SC [13,14]. In particular, among the conventional BCS-type oxide superconductors, hole-doped bismuthate $BaPb_{1-x}Bi_xO_3$ (BPBO) at the optimal doping point ($x = 0.25$) exhibits a relatively high superconducting transition temperature ($T_c \sim 11$ K) [13,15]. Moreover, BPBO is an isotropic superconductor that has nonmagnetic properties unlike cuprate superconductors. In bulk BPBO, structural disorder [16–19] and strong electron-phonon coupling [20–24] have been studied intensively by researchers aiming to characterize its SC, such as superconductor-to-insulator transition (SIT) and T_c modulation. In this respect, coherent-strained BPBO films could contribute to elucidating unresolved issues regarding its SC, such as electron-phonon coupling controlled by dimensionality [25] and the hidden structural disorder of thin-film states. Furthermore, recent observation of emergent two-dimensional superconductivity between $BaBiO_3$ and $BaPbO_3$ bilayer hosts new interest to the interface of BPBO [26], which requires coherent-strained BPBO thin film with a well-defined interface.

The superconducting BPBO films were reported earlier [27,28], but their polycrystalline structures with grain boundaries hindered the study on the physical properties of BPBO films [28]. With the synthesis of single-crystalline BPBO films, the precise physical properties of BPBO films have been investigated including optical and transport properties [29,30]. However, strain engineering or understanding on the interface of BPBO films have been limited due to the large lattice mismatches between pseudocubic BPBO ($a_{pc} \sim 4.300$ Å) and widely used perovskite substrates, such as $SrTiO_3$ [(STO), $a \sim 3.905$ Å], resulting in lattice mismatches up to ~10.1%. Under large lattice mismatches, coherent growth is limited [31–33] and misfit dislocations or reconstructed interface layers [34] are easily formed as a mechanism to release strain

*Corresponding author: cshyoung@cau.ac.kr
†twnoh@snu.ac.kr

energy. Coherent-strained films can be grown by decreasing the lattice mismatch. The high-quality BPBO films on $LaLuO_3$ substrate ($a_{pc} \sim 4.187$ Å) exhibited the reduced lattice mismatch down to 2.7%, but the coherent-strained structure was sustained only up to 4.5 nm [35]. Below the thickness, BPBO films did not exhibit superconducting behavior. To date, no direct experimental observations of reconstructed interfaces or of superconducting coherent-strained films thicker than the bulk superconducting coherence length ($\xi \sim 7.6$ nm) [36] are available for BPBO films.

In this paper, we fabricated BPBO films grown on STO substrates with and without a $BaCeO_3$(BCO)/$BaZrO_3$(BZO) buffer layer [37] using pulsed laser deposition (PLD). We characterized the hidden interface structure of BPBO films under large lattice mismatches using high-resolution transmission electron microscopy (HRTEM) and grazing-incidence in-plane x-ray diffraction (GIXRD) measurements. Using the buffer layer, we were able to decrease the lattice mismatch from ~10.1% to ~0.8%, leading to coherent-strained BPBO films without structurally modified interface layers. Remarkably, our BPBO films sustained coherent strain up to 10 nm ($>\xi$) and exhibited SC. The coherent-strained BPBO films exhibited higher T_c than relaxed BPBO films. Our results contribute to control of the interfacial structures of BPBO films and exploration of the emergent properties of BPBO-based superconducting devices.

II. EXPERIMENTS

We grew optimally doped BPBO films and BCO/BZO buffer layers on atomically flat TiO_2-terminated STO (001) substrates (see Fig. S1 in the Supplemental Material [38]) using a PLD system with a KrF excimer laser (LPXpro 210; Coherent, Inc.). The BPBO films were grown under an oxygen partial pressure of 100 mTorr with a laser frequency of 3 to 4 Hz and a laser fluence of 0.6 J/cm^2. During deposition, the temperature of the substrate was maintained at 500 °C. After deposition, the samples were cooled at 30 °C/min under an oxygen partial pressure of 100 mTorr. The resistivity of the BPBO films was measured using a four-probe method with a physical property measurement system (Quantum Design). The thickness was measured by x-ray reflectivity and/or HRTEM.

X-ray diffraction [(XRD); Bruker AXS D8 with a Vantec line-detector] with a Cu K α-1 source ($\lambda = 1.5406$ Å) and atomic force microscopy [(AFM); Cypher; Asylum] were performed at room temperature under ambient pressure. For detailed structural analyses of BPBO films and the interface, synchrotron-based XRD was performed using Huber six-circle diffractometers at Sector 3A of the Pohang Light Source (South Korea). Note that GIXRD was carried out to monitor the depth profile of in-plane lattice parameters.

The crystal structure analysis of BPBO films on STO substrates (BPBO/STO) and BPBO films with BCO/BZO buffer layers (BPBO/buffer) was performed by HRTEM. Here, BPBO/buffer represents BPBO/BCO/BZO/STO or BPBO/buffer/STO. Cross-sectional HRTEM specimens were prepared by focused ion-beam milling (Helios 650 FIB, FEI) and further thinned by focused Ar-ion milling (NanoMill 1040, Fischione). HRTEM images were obtained with a JEOL JEM-2100F equipped with a field emission gun at an acceleration voltage of 200 kV. The electron-beam exposure time of BPBO/STO was 0.3 s and that of BPBO/buffer was 0.5 s. Since BPBO thin films are easily damaged by the electron beam, the perfect crystal structure was destroyed in a few seconds. Note that BPBO/STO was more easily damaged by the electron beam than BPBO/buffer. To visualize the interface region clearly, we plotted the in-plane strain map ($\varepsilon_{xx} = \frac{\partial u}{\partial x}$, where u is the local displacement of the reciprocal lattice vector) of both BPBO/STO and BPBO/buffer using geometric phase analysis (GPA) algorithm [39] by STRAIN++ software. The GPA method can address local relative lattice displacement or deformation from the lattice fringes of periodic reference crystals in real space using filtering in Fourier space. The reference crystal positions of the GPA method were set to the high crystalline BPBO regions, which were far from the interface. For all images, the horizontal and vertical lines represent the $[100]_{pc}$ and $[001]_{pc}$ orientations, respectively.

III. RESULTS AND DISCUSSION

Figures 1(a) and 1(b) show schematics of BPBO/STO and BPBO/buffer, respectively. As indicated in Figs. 1(a) and 1(b), the pseudocubic in-plane lattice parameters of each perovskite layer are represented by a_{pc}. The a_{pc} was determined by reciprocal space mapping (RSM) of high-resolution XRD around STO {103} diffraction as shown in Figs. 1(c) and 1(d). Note that H (or K) and L represent the in-plane and out-of-plane relative lattice units (r.l.u.) of the STO substrate, respectively. Figures 1(c) and 1(d) clearly demonstrate that the in-plane directions in the pseudocubic BPBO structure are the same as in the STO substrate. We observed little variation in the H (or K) and L values of BPBO films in the RSM with four different azimuthal φ angles. This indicates that the BPBO film has close to tetragonal symmetry or a monoclinic (or distorted orthorhombic) structure with four domains [40–42] in the cases of both BPBO/STO and BPBO/buffer.

As shown in Fig. 1(c), BPBO/STO exhibits a fully relaxed structure with $a_{pc} = 4.300$ Å, under a large lattice mismatch of approximately 10.1% (compressive). The fully relaxed structure of the BPBO film is quite similar to that of the $BaBiO_3$ film grown on the STO substrate (BBO/STO) [41]. As shown in Fig. 1(d), however, the BPBO/buffer exhibited coherent-strained structure with $a_{pc} = 4.335$ Å. The BCO/BZO buffer layer significantly decreased the lattice mismatch from 10.1% (for BPBO/STO) to 0.8%, which led to tensile strain. We confirmed that the buffer layer thickness does not affect to the strain on the BPBO film or superconductivity (see Fig. S2 in the Supplemental Material [38]). The thickness of the coherent-strained BPBO film was approximately 10 nm, which was comparable to the bulk coherence length ($\xi \sim 7.6$ nm) [36] or its film coherence length (see Fig. S3 in the Supplemental Material [38]).

As shown in Figs. 1 and 2(a), both the RSM and the 2θ-ω scans indicate that our BPBO/STO and BPBO/buffer were well-ordered single-crystal-like BPBO films along the (001) orientation. In Fig. 2(a), the $(002)_{pc}$ diffraction peaks of the BPBO film and the buffer BZO layer in the BPBO/buffer interfere with each other due to the small differences between

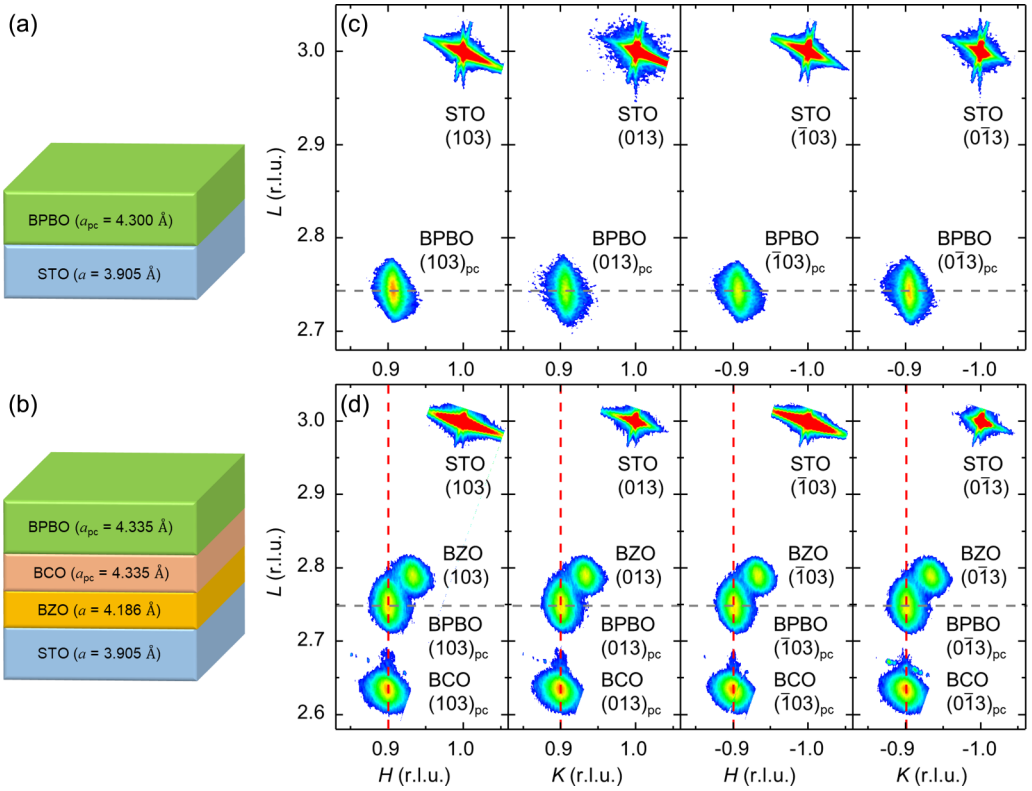

FIG. 1. (a) and (b) Simple schematics of the $BaPb_{0.75}Bi_{0.25}O_3$ film on (a) a $SrTiO_3$ substrate (BPBO/STO, lattice mismatch ∼10.1%) and on (b) a $BaCeO_3$(BCO)/$BaZrO_3$(BZO) buffer layer (BPBO/buffer, lattice mismatch ∼0.8%). The in-plane lattice parameters (a or a_{pc}) of each layer were determined by RSM. a_{pc} represents the pseudocubic in-plane lattice parameters of each layer. (c) RSM around $\{103\}_{pc}$ diffractions for a fully relaxed BPBO/STO and (d) a fully strained (∼0.8%) BPBO/buffer, respectively. H and L represent the r.l.u. of the STO in the in-plane and out-of-plane directions, respectively. The vertical dotted lines indicate that the BPBO layer was fully strained on the BCO layer. The horizontal dotted lines denote the L values of the BPBO peaks.

the lattice parameters. Figure 2(b) shows the $(002)_{pc}$ rocking curves of BPBO films in both BPBO/STO and BPBO/buffer. These were high crystalline BPBO films with a relatively sharp full width at half maximum compared to the STO substrate of 0.010° (see Fig. S1(a) in the Supplemental Material [38]). As shown in Figs. 2(c) and 2(d), representative AFM images of both samples confirm the smooth surfaces with clear step and terrace formations and roughness values smaller than 0.5 nm. These are consistent with the clear Kiessig fringes shown in the x-ray 2θ-ω scans.

To gain further insight into the coherent growth, we investigated the crystal structures of both BPBO/STO and BPBO/buffer samples using HRTEM. Figure 3(a) is a representative HRTEM image of the BPBO/STO in the $[100]_{pc}$ zone axis. Figure 3(b) is the enlarged interface area (red dotted line) from Fig. 3(a). In BPBO/STO, the BPBO film exhibited good crystallinity in the region far from the substrate, whereas noteworthy features of the deformed structure appear at the interface between BPBO and STO. In Fig. 3(c), the interface structure of BPBO/STO was emphasized by the in-plane strain map (ε_{xx}) of the selected area in Fig. 3(b) using a GPA algorithm [39]. In BPBO/STO, the film's structure near the interface at 1 to 2 nm is strongly deformed and exhibited interfacial imperfections under large compressive strain. The interface layer is similar to that previously reported for the BBO/STO heterostructures [43]. However, the ε_{xx} values in the BPBO region above the few nanometers from the interface are represented by a relatively uniform color, indicating that the BPBO film above the interface region quickly relaxed and exhibited a high-quality structure, which is consistent with the rocking curves of the BPBO film shown in Fig. 2(b).

In the case of the BPBO/buffer, we confirmed the high-quality and coherent-strained BPBO film structure without any deformed interface layer, according to the HRTEM image shown in Figs. 3(d) and 3(e). The ε_{xx} strain map of the BPBO/buffer was quite similar to that of BPBO/STO far from the interface region. Interestingly, the ε_{xx} strain map of the interface region of the BPBO/buffer in Fig. 3(f) shows less strain variation than that of BPBO/STO near the interface (local lattice displacement of around ± 20%) in Fig. 3(c). As shown in Figs. 3(e) and 3(f), the BPBO/buffer had good crystallinity without stacking faults or defects especially at the interface. This indicates that we achieved coherent-strained BPBO films without a deformed interface layer by reducing the lattice mismatch from 10.1% to 0.8%.

Although the GPA method based on HRTEM can reveal the existence (or absence) of a deformed interface layer, it remains challenging to acquire detailed structural information or the possibility of chemical intermixing at the interfaces of BPBO heterostructures. As bismuthate films are extremely vulnerable to electron-beam exposure [44,45], the scope for obtaining scanning HRTEM images with atomic resolution

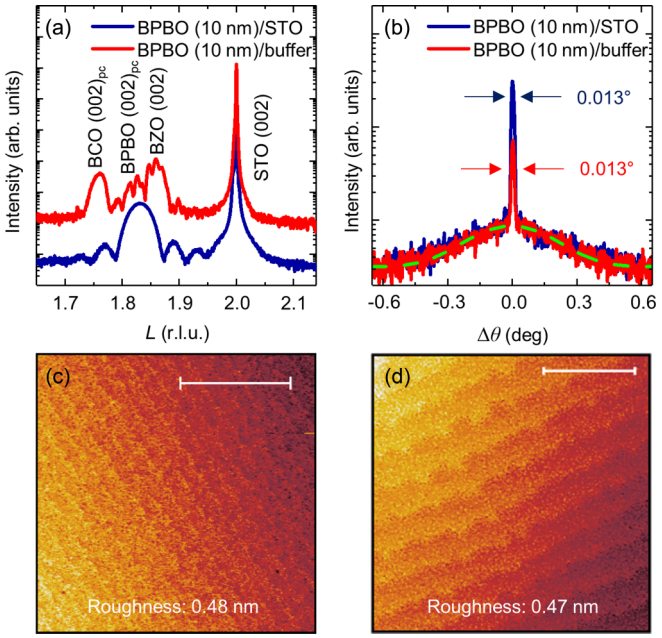

FIG. 2. (a) XRD 2θ-ω scans of the BPBO/STO and BPBO/buffer around the $(002)_{pc}$ diffraction peak. (b) Rocking curves of BPBO $(002)_{pc}$ diffraction for BPBO/STO and the BPBO/buffer. AFM images of (c) BPBO/STO and (d) the BPBO/buffer, respectively. The white scale bars in (c) and (d) represent 2 and 1 μm, respectively.

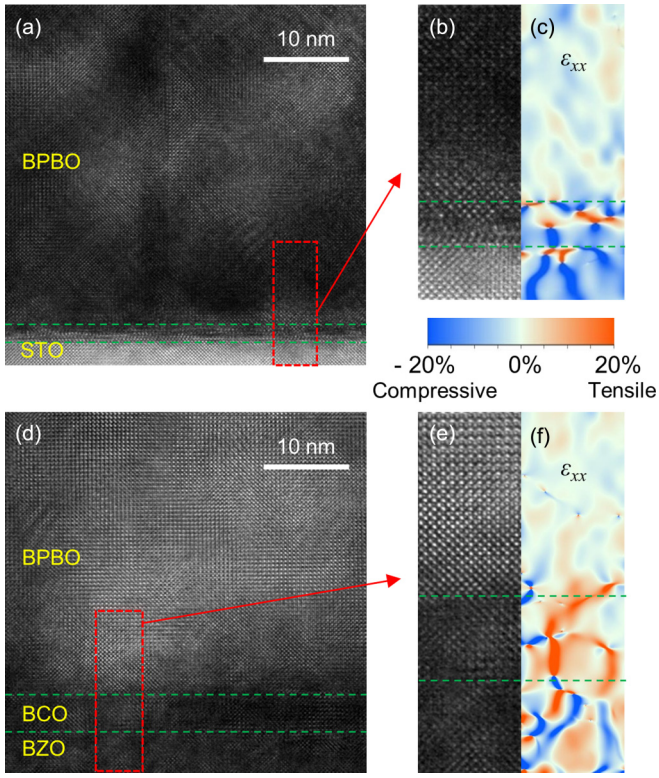

FIG. 3. HRTEM images of BPBO/STO and the BPBO/buffer. (a) HRTEM image of BPBO/STO. (b) Enlarged image of the interface from (a). In BPBO/STO, the interface layer exists between BPBO and STO. (c) In-plane strain (ε_{xx}) map converted by GPA for BPBO/STO. ε_{xx} represents the local relative lattice deformation in the in-plane direction. (d) HRTEM image of the BPBO/buffer. The thickness of the BCO layer (t_{BCO}) and BZO layer (t_{BZO}) were 5 nm for both. (e) Enlarged image of the interface from (d). (f) The ε_{xx} map converted by GPA for the BPBO/buffer.

is limited. As an alternative, we propose synchrotron-based GIXRD measurements [46] combined with RSM. GIXRD is a powerful method for investigating the depth profile of in-plane lattice parameters of both films and substrates [47]. Note that α, $2\theta\chi$, and φ are the grazing-incidence angle, the horizontal angle of the diffracted x-ray beam, and the azimuthal angle of the incidence x-ray beam, respectively. The x-ray penetration depth (d_X) can be calculated as a function of α, which is larger than the total reflection critical angle ($\alpha_c \sim 0.2$–0.3°) [48].

Figures 4(a) and 4(b) show schematics of GIXRD and GIXRD measurement around the in-plane $(200)_{pc}$ diffraction peak of BPBO/STO as a function of d_X. Note that the thickness of the BPBO film (t_{BPBO}) was approximately 10 nm, i.e., $t_{BPBO} = 10$ nm, for both BPBO/STO and BPBO/buffer. As shown in Fig. 4(b), we observed two distinguishable a_{pc} values, corresponding to $L \sim 1.82$ and $L \sim 1.91$. The peak measured at $L \sim 1.91$, highlighted by the orange area, is not relevant to the relaxed BPBO film ($L \sim 1.82$) or the STO substrate ($L \sim 2$). Considering that the intensity of the $L \sim 1.91$ peaks was significantly suppressed at $d_X \sim 6$ nm compared to the fully penetrated x-ray ($d_X \sim 22$ nm), the $L \sim 1.91$ peak is estimated to have come from the film-substrate interface. Based on the HRTEM images in Fig. 3, we can demonstrate that the $L \sim 1.91$ peak corresponds to the interface layer structure.

It is surprising that the interface layer in the BPBO/STO heterostructure has a unique structure that differs completely from those of both the BPBO film and the STO substrate. When the lattice mismatch is larger than 7%, coherent growth is difficult to obtain, but epitaxial growth can sometimes be obtained by reducing the residual strain *via* domain-matching epitaxy [33]. In domain-matching epitaxy, the residual strain can be calculated as $\varepsilon_r = (ma_f/na_s) - 1$: where a_f and a_s are the in-plane lattice parameters for the film and substrate, respectively, whereas m and n are proper integers for domain-matching epitaxy. For example, in the BPBO/STO heterostructure, the residual strain ε_r can be calculated as -0.9% [e.g., $(m \times 4.300\,\text{Å})/(n \times 3.905\,\text{Å}) - 1 \sim -0.9\%$, where $m = 9$ and $n = 10$]. However, the interface layer in the BPBO/STO heterostructure seems to have been reconstructed to minimize the strain energy at the two boundaries (i.e., BPBO/interface layer and interface layer/STO) rather than at a single boundary (i.e., BPBO/STO) as shown in Fig. 4(c). We emphasize that the in-plane lattice parameters of the interface layer ($a_{pc} = 4.090$ Å) were relatively similar to the middle value of the in-plane lattice parameter between the fully relaxed BPBO film and the STO substrate. Combined with the GIXRD and RSM around the $(202)_{pc}$ diffraction peak in Fig. 4(d), we confirmed the details of the lattice parameters of the interface layer structure. These were reconstructed with distinguishable lattice parameters ($a_{pc} = b_{pc} = 4.090$, $c_{pc} = 4.414$ Å) as listed in Table I. In this case, the domain-matching epitaxy units can be modified (e.g., $\varepsilon_r \sim -0.5\%$, where $m = 19$, $n = 20$).

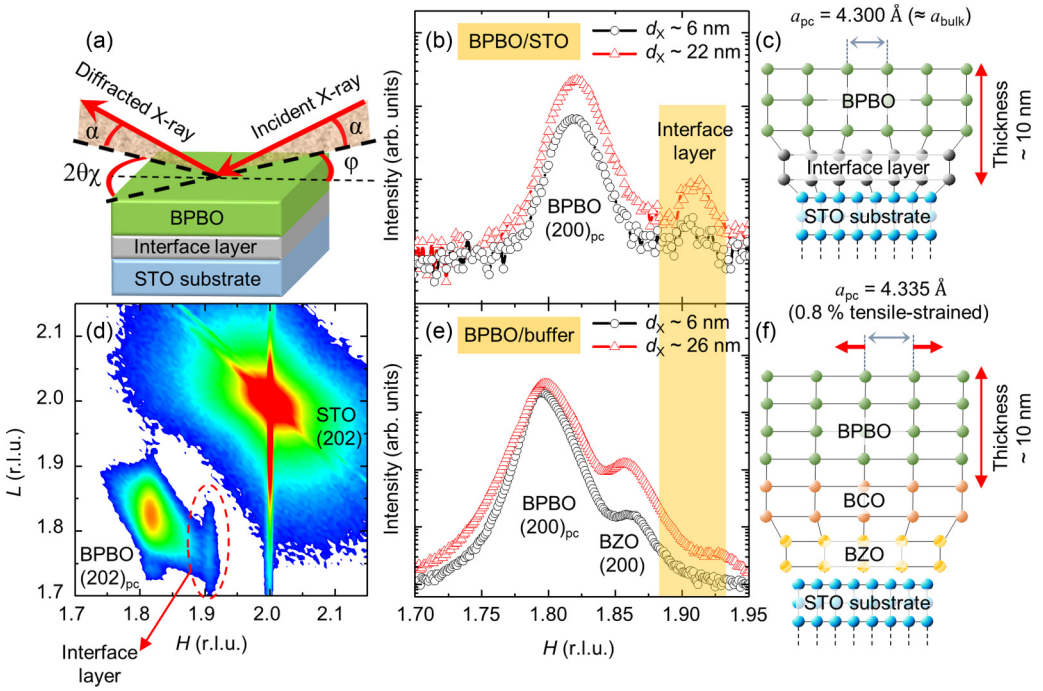

FIG. 4. The interfacial structure of BPBO films detected by GIXRD and RSM. (a) A schematic of GIXRD. The $2\theta\chi$ and φ represent the horizontal detector angle and azimuthal angle, respectively. α represents the incident grazing angle. As α is increased, the x-ray penetration depth d_X goes larger. (b) GIXRD measurements around $(200)_{pc}$ diffractions of BPBO/STO. Vertical orange shadow emphasizes the interface layer peak. (c) A schematic of the BPBO/STO. The structure of BPBO and the interface layer exhibit strain relaxation within a very few nanometers for domain matching. (d) RSM around $(202)_{pc}$ diffraction of the BPBO/STO. Interface layer peak is located beside the BPBO peak. (e) GIXRD measurements around $(200)_{pc}$ diffractions of the BPBO/buffer. (f) A schematic for the BPBO/buffer. The BPBO film exhibits coherent growth on the buffer layer under tensile strain (~0.8%).

If the interface layer in the BPBO/buffer was not reconstructed due to the small lattice mismatch (~0.8%), there would be no observable additional peak at $L \sim 1.91$ in the GIXRD results. As shown in Fig. 4(e), the GIXRD measurement of the BPBO/buffer with $t_{BPBO} = 10$ nm confirms that the interface layer peak disappeared as expected. Note that the BPBO peak and the BCO peak overlap perfectly because they have the same in-plane lattice parameters (see Table I). This result indicates that the BPBO film was fully coherent strained on the BCO layer as shown in Fig. 4(f). The small dependence of a_{pc} on the various values of d_X implies that the BPBO film grew coherently on the buffer layer (see Fig. S4 in the Supplemental Material [38]). The a_{pc} of the coherent-strained BPBO film is different from that of the relaxed BPBO/STO as shown in Table I ($a_{pc} = b_{pc} = 4.335$, $c_{pc} = 4.265$ Å). This implies that we engineered the interfaces of the BPBO-based heterostructures with well-controlled buffer layers.

TABLE I. In-plane and out-of-plane lattice parameters of each layers of both BPBO/STO and BPBO/buffer samples in (pseudo)cubic notation obtained by x-ray scattering measurements. Here, t_{BPBO}, t_{BCO}, and t_{BZO} were 10, 15, and 11 nm, respectively.

		a_{pc} (Å)	b_{pc} (Å)	c_{pc} (Å)
	BPBO	4.300	4.300	4.271
$BPBO/SrTiO_3$	Interface layer	4.090	4.090	4.414
	$SrTiO_3$ (bulk)	3.905	3.905	3.905
	BPBO	4.335	4.335	4.265
BPBO/buffer	$BaCeO_3$	4.335	4.335	4.444
	$BaZrO_3$	4.186	4.186	4.200
	$SrTiO_3$ (bulk)	3.905	3.905	3.905

To elucidate the relationship between the interface layer and the functionality, we took temperature-dependent resistivity (ρ) measurements of fully relaxed BPBO/STO and coherent-strained BPBO/buffer samples as shown in Fig. 5(a). The inset shows the low-temperature region where the superconducting transition occurs. Note that T_c is defined as having half the resistivity of the normal state. In particular, the BPBO/buffer exhibits a superconducting transition at around 6.8 K. We emphasize that we developed a method to create superconducting BPBO films with coherent strain *via* interface engineering. Furthermore, the coherent-strained BPBO film exhibited different T_c's, which is higher than the relaxed BPBO/STO (~6.1 K).

T_c difference between BPBO/buffer and BPBO/STO can be understood in terms of the disorder-superconductivity interaction [18,35]. In superconducting films, disorder causes the SIT, resulting in the changes in T_c and ρ [49–53]. The structural disorder is one of the possible origins of T_c change [18] in BPBO. However, we found that the crystallinity of relaxed BPBO films above the interface in BPBO/STO is quite similar to that of the coherent-strained BPBO film in the BPBO/buffer as shown in Fig. 2(b). Therefore, crystallinity itself is not a plausible explanation for the enhancement of T_c in the BPBO/buffer. Alternatively, the T_c enhancement in the BPBO/buffer can be understood based on electrical transport

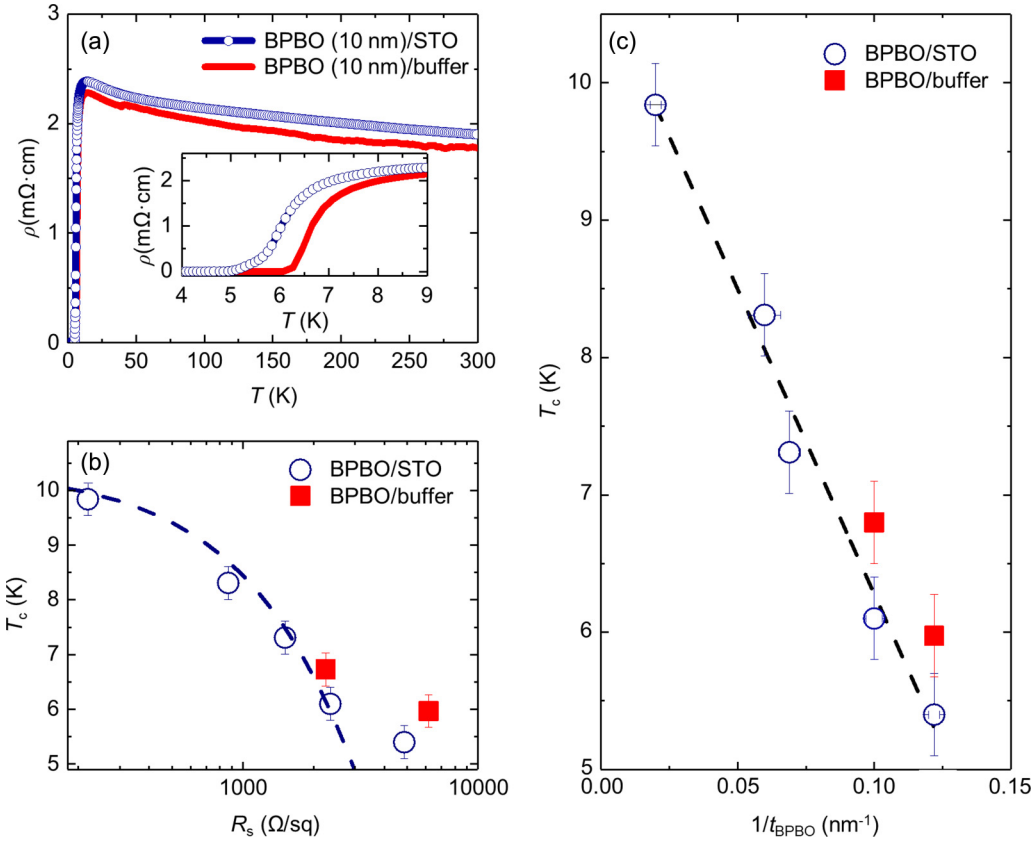

FIG. 5. Superconducting transition temperature (T_c) of BPBO films. (a) Temperature-dependent resistivity (ρ) measurement of BPBO/STO and the BPBO/buffer with $t_{\mathrm{BPBO}} = 10$ nm. The inset shows the low-temperature region near T_c. The BPBO/buffer exhibits higher T_c than BPBO/STO under a given t_{BPBO}. (b) T_c vs sheet resistance (R_s) graph. The dashed blue curve represents the fitting line for BPBO/STO based on the Finkel'stein model. (c) T_c vs $1/t_{\mathrm{BPBO}}$ plot. The BPBO/buffer exhibits higher T_c than BPBO/STO due to the increased effective t_{BPBO}.

measurements. It is known that T_c is effectively tuned by sheet resistance (R_s) or film thickness [51], which is explained by quantum size effect [25,54] or the increase in Coulomb interaction [52,55]. Similarly, the superconducting behavior of BPBO/STO is associated with R_s or thickness, and the SIT could occur at $t_{\mathrm{BPBO}} \sim 5$ nm [35]. Motivated by this as shown in Fig. 5(b), we plotted T_c of BPBO films as a function of R_s (taken at 20 K). The dashed blue curve is the fitting results based on the Finkel'stein model for BPBO/STO [52]. Note that the Finkel'stein model can describe the T_c suppression in terms of R_s in homogeneously disordered superconducting films by the following renormalization-group equation:

$$T_c = T_c^0 e^{-(1/\gamma)}\left[\left(1+\frac{(r/2)^{1/2}}{\gamma - r/4}\right)\left(1-\frac{(r/2)^{1/2}}{\gamma - r/4}\right)^{-1}\right]^{1/\sqrt{2r}},$$

where T_c^0 is the bulk superconducting transition temperature, $\gamma = 1/\ln(k_B T_c^0 \tau/\hbar)$ and $r = R_s/(2\pi^2\hbar/e^2)$. Here, τ is the elastic-scattering time. The Finkel'stein model fitted well on BPBO/STO and the BPBO/buffer in the smaller R_s region ($t_{\mathrm{BPBO}} > 10$ nm) as reported before [35], but we were not able to address the disorder of the BPBO/buffer in the higher R_s region ($t_{\mathrm{BPBO}} < 10$ nm). Rather than R_s, we found that the thickness can be more proper parameter to tune T_c of the BPBO films, related to the existence or (absence) of the interface layer. If the interface layer of the BPBO/STO did not exhibit a superconducting state, the effective thickness of the BPBO/STO would be reduced, and T_c would be modulated. As shown in Fig. 5(c), we systematically investigated T_c of the BPBO film as a function of the inverse of thickness $1/t_{\mathrm{BPBO}}$ [53]. The dashed black line represents the linear least-squares fitting line of the BPBO/STO. We found that T_c decreased with increasing in $1/t_{\mathrm{BPBO}}$ (decreasing in t_{BPBO}), which is consistent with the behavior of the BPBO film or other disordered superconducting films [35,51,53]. As shown in Fig. 5(c), if BPBO/STO exhibits the same T_c with that of the BPBO/buffer, the BPBO/STO should be 1 to 2-nm thicker than the BPBO/buffer. Considering the thickness of the interface layer in BPBO/STO [Fig. 3(b)], this result implies that the interface layer of BPBO/STO might not exhibit superconductivity. From this, we propose that the absence of an interface layer in the BPBO/buffer would increase the effective t_{BPBO} under a given film thickness and would contribute to the enhanced T_c compared to BPBO/STO. To address the precise superconducting effective thickness, further transport measurements would be needed [56].

Not only the disorder, but also the strain could play important roles in determining T_c of BPBO films. Strain can be used to tune the lattice symmetry, density of states at the Fermi level [57], or octahedral distortion, which is closely related to the electron-phonon coupling [31] and corresponding T_c in Migdal-Eliashberg theory. However, little has been reported on the effect of strain on BPBO films due to a lack of high-quality BPBO films with coherent strain. Hence, our

coherent-strained film can offer a platform for strain engineering on BPBO films, which promises fruitful applications with bismuthate-based topological quantum devices.

IV. SUMMARY

To summarize, we achieved coherent-strained superconducting BPBO films by interface engineering with the buffer layer, reducing the lattice mismatch from 10.1% to 0.8%. Without the buffer layer, we observed that the BPBO/STO heterostructure exhibited a reconstructed interface layer due to the large lattice mismatch. The interface layer had completely different lattice parameters compared to the fully relaxed BPBO film or STO substrate. Using the buffer layer, we were able to control the interface of the BPBO heterostructure with an atomically sharp interface. The BPBO/buffer exhibited higher T_c than that of BPBO/STO, which implies that the interface layer would be not superconducting such that the effective t_{BPBO} increased in the BPBO/buffer. Our paper reveals the interface structure of BPBO films and suggests a way to control the interface, thus, contributing to the fabrication of BPBO-based next-generation devices.

ACKNOWLEDGMENTS

This work was supported by the Institute for Basic Science in Korea (Grant No. IBS-R009-D1) and the Core-to-Core program "Oxide Superspin." S.H.C. was supported by Basic Science Research Programs through the National Research Foundation of Korea (Grants No. NRF-2019K1A3A7A09033393 and No. 2018R1D1A1B07046396).

The authors declare no competing financial interests.

[1] A. Ohtomo and H. Y. Hwang, Nature (London) **427**, 423 (2004).
[2] N. Reyren, S. Thiel, A. D. Caviglia, L. F. Kourkoutis, G. Hammerl, C. Richter, C. W. Schneider, T. Kopp, A.-S. Rüetschi, D. Jaccard, M. Gabay, D. A. Muller, J.-M. Triscone, and J. Mannhart, Science **317**, 1196 (2007).
[3] A. Gozar, G. Logvenov, L. F. Kourkoutis, A. T. Bollinger, L. A. Giannuzzi, D. A. Muller, and I. Bozovic, Nature (London) **455**, 782 (2008).
[4] J. Wang, J. B. Neaton, H. Zheng, V. Nagarajan, S. B. Ogale, B. Liu, D. Viehland, V. Vaithyanathan, D. G. Schlom, U. V. Waghmare, N. A. Spaldin, K. M. Rabe, M. Wuttig, and R. Ramesh, Science **299**, 1719 (2003).
[5] A. Brinkman, M. Huijben, M. Van Zalk, J. Huijben, U. Zeitler, J. C. Maan, W. G. Van Der Wiel, G. Rijnders, D. H. A. Blank, and H. Hilgenkamp, Nat. Mater. **6**, 493 (2007).
[6] H. Jin, S. H. Rhim, J. Im, and A. J. Freeman, Sci. Rep. **3**, 1651 (2013).
[7] B. Yan, M. Jansen, and C. Felser, Nat. Phys. **9**, 709 (2013).
[8] G. Li, B. Yan, R. Thomale, and W. Hanke, Sci. Rep. **5**, 10435 (2015).
[9] B. Pang, L. Zhang, Y. B. Chen, J. Zhou, S. Yao, S. Zhang, and Y. Chen, ACS Appl. Mater. Interfaces **9**, 3201 (2017).
[10] L. Wang, Q. Feng, Y. Kim, R. Kim, K. H. Lee, S. D. Pollard, Y. J. Shin, H. Zhou, W. Peng, D. Lee, W. Meng, H. Yang, J. H. Han, M. Kim, Q. Lu, and T. W. Noh, Nat. Mater. **17**, 1087 (2018).
[11] M. Uchida and M. Kawasaki, and J. Phys. D: Appl. Phys. **51**, 143001 (2018).
[12] L. Fu and C. L. Kane, Phys. Rev. Lett. **100**, 096407 (2008).
[13] A. W. Sleight, J. L. Gillson, and P. E. Bierstedt, Solid State Commun. **17**, 27 (1975).
[14] R. J. Cava, B. Batlogg, J. J. Krajewski, R. Farrow, L. W. Rupp, Jr., A. E. White, K. Short, W. F. Peck, and T. Kometani, Nature (London) **332**, 814 (1988).
[15] A. W. Sleight, Physica C **514**, 152 (2015).
[16] D. T. Marx, P. G. Radaelli, J. D. Jorgensen, R. L. Hitterman, D. G. Hinks, S. Pei, and B. Dabrowski, Phys. Rev. B **46**, 1144 (1992).
[17] E. Climent-Pascual, N. Ni, S. Jia, Q. Huang, and R. J. Cava, Phys. Rev. B **83**, 174512 (2011).
[18] K. Luna, P. Giraldo-Gallo, T. Geballe, I. Fisher, and M. Beasley, Phys. Rev. Lett. **113**, 177004 (2014).
[19] P. Giraldo-Gallo, Y. Zhang, C. Parra, H. C. Manoharan, M. R. Beasley, T. H. Geballe, M. J. Kramer, and I. R. Fisher, Nat. Commun. **6**, 8231 (2015).
[20] K. Kitazawa, M. Naito, T. Itoh, and S. Tanaka, J. Phys. Soc. Jpn. **54**, 2682 (1985).
[21] T. M. Rice and L. Sneddon, Phys. Rev. Lett. **47**, 689 (1981).
[22] S. Sugai, Solid State Commun. **72**, 1187 (1989).
[23] C. Franchini, G. Kresse, and R. Podloucky, Phys. Rev. Lett. **102**, 256402 (2009).
[24] Z. P. Yin, A. Kutepov, and G. Kotliar, Phys. Rev. X **3**, 021011 (2013).
[25] Y. Guo, Y. F. Zhang, X. Y. Bao, T. Z. Han, Z. Tang, L.-X. Zhang, W. G. Zhu, E. G. Wang, Q. Niu, Z. Q. Qiu, J.-F. Jia, Z.-X. Zhao, and Q.-K. Xue, Science **306**, 1915 (2004).
[26] B. Meir, S. Gorol, T. Kopp, and G. Hammerl, Phys. Rev. B **96**, 100507(R) (2017).
[27] L. R. Gilbert, R. Messier, and R. Roy, Thin Solid Films, **54**, 129 (1978).
[28] M. Suzuki, Y. Enomoto, and T. Murakami, J. Appl. Phys. **56**, 2083 (1984).
[29] M. Suzuki, Jpn. J. Appl. Phys. **32**, 2640 (1993).
[30] K. H. Kim, C. U. Jung, T. W. Noh, and S. C. Kim, Phys. Rev. B **55**, 15393 (1997).
[31] J. Varignon, J. Santamaria, and M. Bibes, Phys. Rev. Lett. **122**, 116401 (2019).
[32] T. Zheleva, K. Jagannadham, and J. Narayan, J. Appl. Phys. **75**, 860 (1994).
[33] J. Narayan and B. C. Larson, J. Appl. Phys. **93**, 278 (2003).
[34] Y. Zhu, A. Chen, H. Zhou, W. Zhang, J. Narayan, J. L. MacManus-Driscoll, Q. Jia, and H. Wang, APL Mater. **1**, 050702 (2013).
[35] D. T. Harris, N. Campbell, R. Uecker, M. Brützam, D. G. Schlom, A. Levchenko, M. S. Rzchowski, and C.-B. Eom, Phys. Rev. Mater. **2**, 041801 (2018).
[36] S. Uchida, K. Kitazawa, and S. Tanaka, Phase Transitions **8**, 95 (1987).
[37] H. G. Lee, Y. Kim, S. Hwang, G. Kim, T. D. Kang, M. Kim, M. Kim, and T. W. Noh, APL Mater. **4**, 126106 (2016).

[38] See Supplemental Material at https://link.aps.org/supplemental/10.1103/PhysRevMaterials.3.113606 for substrate characterization, x-ray diffraction, reciprocal space mapping, depth-dependent in-plane lattice constant, low-temperature resistivity, and upper critical field (H_{c2}) of BPBO films.

[39] M. J. Hÿtch, E. Snoeck, and R. Kilaas, Ultramicroscopy **74**, 131 (1998).

[40] S. H. Chang, Y. J. Chang, S. Y. Jang, D. W. Jeong, C. U. Jung, Y. J. Kim, J. S. Chung, and T. W. Noh, Phys. Rev. B **84**, 104101 (2011).

[41] G. Kim, M. Neumann, M. Kim, M. D. Le, T. D. Kang, and T. W. Noh, Phys. Rev. Lett. **115**, 226402 (2015).

[42] R. Gao, Y. Dong, H. Xu, H. Zhou, Y. Yuan, V. Gopalan, C. Gao, D. D. Fong, Z. Chen, Z. Luo, and L. W. Martin, ACS Appl. Mater. Interfaces **8**, 14871 (2016).

[43] M. Zapf, M. Stübinger, L. Jin, M. Kamp, F. Pfaff, A. Lubk, B. Büchner, M. Sing, and R. Claessen, Appl. Phys. Lett. **112**, 141601 (2018).

[44] H. G. Lee, R. Kim, J. Kim, M. Kim, T. H. Kim, S. Lee, and T. W. Noh, APL Mater. **6**, 016107 (2018).

[45] D. T. Harris, N. Cambell, C. Di, J.-M. Park, L. Luo, H. Zhou, G.-Y. Kim, S.-Y. Choi, J. Wang, M. S. Rzchowski, and C.-B. Eom, arXiv:1812.08589.

[46] W. C. Marra, P. Eisenberger, and A. Y. Cho, J. Appl. Phys. **50**, 6927 (1979).

[47] D. Lee, A. Yoon, S. Y. Jang, J. G. Yoon, J. S. Chung, M. Kim, J. F. Scott, and T. W. Noh, Phys. Rev. Lett. **107**, 057602 (2011).

[48] A. Thompson, D. Attwood, E. Gullikson, M. Howells, K.-J. Kim, J. Kirz, J. Kortright, I. Lindau, P. Pianatta, A. Robinson, J. Scofield, J. Underwood, D. Vaughan, G. Williams, and H. Winick, *X-ray Data Booklet* (Lawrence Berkeley National Laboratory, University of California, Berkeley, CA, 2001).

[49] A. Shalnikov, Nature (London) **142**, 74 (1938).

[50] Y. Dubi, Y. Meir, and Y. Avishai, Nature (London) **449**, 876 (2007).

[51] Y. Ivry, C. S. Kim, A. E. Dane, D. De Fazio, A. N. McCaughan, K. A. Sunter, Q. Zhao, and K. K. Berggren, Phys. Rev. B **90**, 214515 (2014).

[52] A. M. Finkel'stein, Physica B **197**, 636 (1994).

[53] S. Ezaki, K. Makise, B. Shinozaki, T. Odo, T. Asano, H. Terai, T. Yamashita, S. Miki, and Z. Wang, J. Phys.: Condens. Matter **24**, 475702 (2012).

[54] L. Kang, B. B. Jin, X. Y. Liu, X. Q. Jia, J. Chen, Z. M. Ji, W. W. Xu, P. H. Wu, S. B. Mi, A. Pimenov, Y. J. Wu, and B. G. Wang, J. Appl. Phys. **109**, 033908 (2011).

[55] S. Maekawa and H. Fukuyama, J. Phys. Soc. Japan **51**, 1380 (1982).

[56] N. Reyren, S. Gariglio, A. D. Caviglia, D. Jaccard, T. Schneider, and J.-M. Triscone, Appl. Phys. Lett. **94**, 112506 (2009).

[57] A. Steppke, L. Zhao, M. E. Barber, T. Scaffidi, F. Jerzembeck, H. Rosner, A. S. Gibbs, Y. Maeno, S. H. Simon, A. P. Mackenzie, and C. W. Hicks, Science **355**, eaaf9398 (2017).